arXiv:1607.05583v1 [physics.gen-ph] 5 Jul 2016

A New Viable f(R) Model in the Light of Local Gravity Test and Late-time Cosmology

Akhilesh Nautiyal*[a,b], Sukanta Panda†[b], and Avani Patel‡[b]

[a]Department of Physics, Malaviya National Institute of Technology Jaipur, Jaipur 302 017, India

[b]Department of Physics, Indian Institute of Science Education and Research Bhopal, Bhopal 462 066, India

Abstract

We propose a new model of $f(R)$ gravity containing Arctan function in the lagrangian. We show here that this model satisfies fifth force constraint unlike a similar model [1]. In addition to this, we carry out the fixed point analysis as well as comment on the existence of curvature singularity in this model. The cosmological evolution for this $f(R)$ gravity model is also analyzed in the Freidmann Robertson Walker background. To understand observational significance of the model, cosmological parameters are obtained numerically and compared with those of Lambda cold dark matter (ΛCDM) model. We also scrutinize the model with supernova data.

1 Introduction

Recent progress in the precise measurements of cosmic microwave background anisotropies and observations of type Ia supernovae and large scale structure strongly indicate that our universe, at present, is expanding acceleratingly [2]. If General Relativty is assumed to be a correct theory to explain the large scale structure of the universe then an extra unknown component called dark energy is required to dominate over all other matter in recent times to drive such accelerating expansion. These observations also suggest that the equation of state parameter of unknown source should be negative. The simplest model which accommodates these features and is consistent with most of the observations is ΛCDM model, where Λ represents cosmological constant. The required value of the cosmological constant in order to fit with observations is many orders of magnitude smaller than the value encountered from standard field theoretic arguments [3]. This large discrepancy forces us to look for alternative explanations for dark energy. One of such scenario is to replace the Ricci scalar, R, in Einstein-Hilbert action, by a general function of R, i.e, $f(R)$. For a review on f(R) theories of gravity refer to [4–7].

Dark energy models based on $f(R)$ theories have been developed and studied extensively to realize an accelerating era in recent times. Since observations favor cosmological constant as a best fit dark energy candidate, natural possibility for $f(R)$ model is to construct one that can mimick as an effective cosmological constant today and at the same time it should be distinguishable from ΛCDM model at early times. With this clue many $f(R)$ models were proposed [8–19] which behave as the ΛCDM model at large curvature limit i.e. $f(R) \to R - 2\Lambda$ for $R >> \Lambda$ and $f(R)$ tends to zero as $R \to 0$. The dynamical system analysis of f(R) theories are done in Ref. [20] and these theories are classified according to their fixed points. A new approach for dynamical system analysis of $f(R)$ models is

*akhilesh.phy@mnit.ac.in

†sukanta@iiserb.ac.in

‡avani@iiserb.ac.in

found and applied to few viable models in [21, 22]. Another important issue about $f(R)$ theory is that since it is a modified theory of gravity, it should be put under the test to inquire that it does not spoil the successes of GR at local scales like solar system. In general, all f(R) theories are effective scalar-tensor theories with a potential term. If the mass of the scalar field is order of present hubble parameter then it is difficult to satisfy the local gravity constraints due to the long range fifth force with a large coupling strength. This can be avoided with a mechanism such that mass of the scalar field varies with the background density and as a result fifth force can be very short range force in high density region. This is well known as chameleon mechanism [23–25].

Many $f(R)$ models are also plagued by fatal curvature singularities of various types. The cosmological evolution happens at the minimum of the scalar field potential around which scalar field oscillates. The point of diverging curvature exists near the minimum at a finite potential in many $f(R)$ models [1,26–28]. The finite-time singularity in modified gravity is described in [29–34]. It is also realised that the curvature singularities can be eliminated by adding an extra curvature term to the Lagrangian [11,26]. The curvature singularity can also be seen in an astrophysical object [1,28,35–37]. The extensive investigations of singularities in relativistic stars are done in [38–40].

In Ref. [1], a detailed study of local gravity tests and fixed-point analysis is done for an arctan model proposed in [19]. It turns out that this simple arctam model is ruled out by fifth-force constraint. In this work, we propose a new Arcta model of $f(R)$ gravity extending the model in [19]. We check the viability of the model through local gravity test. In addition to this, we also carry out dynamical system analysis and find the fixed points, for this model following the line of Ref. [20]. Cosmological evolution with this model is also presented by solving FRW equations numerically as described in [41]. The distance modulus calculated in this model is fitted with the supernova data for certain parameters.

This paper progresses as follows. Sec. 2 gives the general idea of the modified ArcTan model and de Sitter points are obtained in Sec. 2.1. Sec. 2.2 discusses the fixed points of the model and their stability. The fifth-force test and its result is explained in Sec. 3. The investigation of curvature singularity is carried out in Sec. 4. Sec. 5 presents cosmological evolution and behaviour of density parameters and equation of state with the given modified ArcTan model. The luminosity distance and distance modulus in this model along with the Union 2 compilation of supernova data [42] is given in Sec. 6. Finally, conclusions are discussed in Sec. 7.

2 A New $f(R)$ Model

In $f(R)$ theory, Hilbert-Einstein action is replaced by a more general action

$$S = \int d^4x\sqrt{-g}\left[\frac{1}{2\kappa^2}f(R) + \mathfrak{L}_m\right], \tag{1}$$

where $f(R)$ is an arbitrary function of Ricci scalar R and $\mathfrak{L}_m$ is usual matter lagrangian. It is more convenient to write the function $f(R)$ as $f(R) = R + F(R)$, where $F(R)$ is an arbitrary function of R. It can be easily seen that one can retain GR and ΛCDM for $F(R) = 0$ and $F(R) = -2\Lambda$ respectively. Another benefit of writing $f(R)$ in this way is that effects of modification to Einstein gravity is more evident and its study becomes simpler. Here, we propose a new model of $f(R)$ theory, slightly modifying arctan model given in [19],

$$F(R) = -\frac{b}{\beta}\arctan(\beta R)^n. \tag{2}$$

Here, b, β and n are positive constants. β has the inverse dimension of Ricci scalar R and it is of the order of inverse of presently observed effective cosmological constant. Note that our model reduces to the arctan model proposed in [19] for $n = 1$. Whenever we write "arctan model" throughout this paper we mean the model in [19]. In Fig.1, the function $-\beta F(R)$ is plotted w.r.t. βR for different values of n. One can see from the Fig.1 that the variations in $\beta F(R)$ occurs only between $R \sim 1 - 5$. Beyond $R \sim 5$, the value of $\beta F(R)$ becomes nearly constant. This behaviour tells us that our model

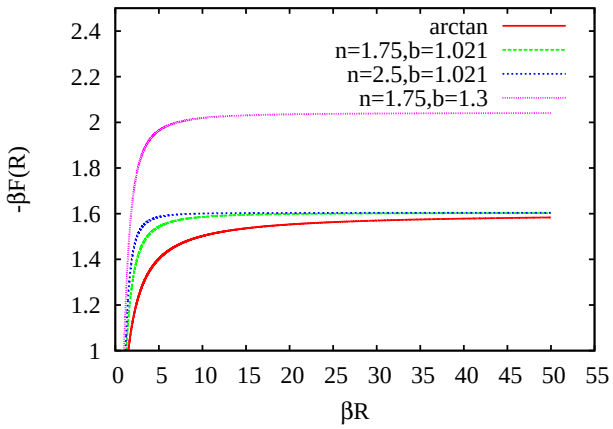

Figure 1: $-\beta F(R)$ Vs. βR. In "arctan" curve $n = 1$ and $b = 1.021$ are taken.

given in Eq. (2) mimics as ΛCDM at high curvature i.e. at $R >> 1/\beta$ and $f(R)$ becomes zero at $R = 0$. Also, notice that the function $F(R)$ increases and becomes constant more rapidly as n increases, which suggests that the value of parameter n should be small enough so that the model can explain correct cosmic history. While keeping n constant, the shape of the curve remains same but its magnitude increases with increasing b.

2.1 Constant Curvature Solution

By varying the action written in Eq. (1) w.r.t. $g_{\mu\nu}$ we obtain the field equation given as,

$$f_{,R}R_{ab} - \frac{1}{2}f g_{ab} - (\nabla_a\nabla_b - g_{ab}\Box)\, f_{,R} = \kappa^2 T_{ab}. \tag{3}$$

Here $\kappa^2 = 8\pi G$ and $\Box = g^{ab}\nabla_a\nabla_b$ is the covariant D'Alambertian. Any quantity with $,R$ in the subscript denotes derivative w.r.t R. Eq. (3) can also be written in the following form by using the expression for Einstein tensor G_{ab}

$$f_{,R}G_{ab} - f_{,RR}\nabla_a\nabla_b R - f_{,RRR}\,(\nabla_a R)\,(\nabla_b R) + g_{ab}\left[\frac{1}{2}\,(Rf_{,R} - f) + f_{RR}\Box R + f_{,RRR}\,(\nabla R)^2\right] = \kappa^2 T_{ab}, \tag{4}$$

where $(\nabla R)^2 = g^{ab}\,(\nabla_a R)\,(\nabla_b R)$. The trace of the above field equation is given by

$$3f_{,RR}(R)\Box R - 2f(R) + Rf_{,R} + 3f_{,RRR}\,(\nabla R)^2 = \kappa^2 T \tag{5}$$

which can be rewritten as

$$\Box R = \frac{1}{3f_{,RR}}\left[\kappa^2 T - 3f_{,RRR}\,(\nabla R)^2 + 2f - Rf_{,R}\right] \tag{6}$$

The constant curvature solution of Eq. (6) in vacuum describes the de Sitter universe. It corresponds to the condition

$$2f(R_d) - R_d f_{,R}(R_d) = 0, \tag{7}$$

having de Sitter point denoted as R_d. A few de Sitter points for different values of n and b are listed in Table1. Though there can be more than one values of R_d which can be solutions of above equation, only stable points are physically true de Sitter points. A de Sitter point R_d is a stable point describing primordial and present vacuum energy dominated epoch if it satisfies the condition $F_{,R}(R_d)/F_{,RR}(R_d) > R_d$. All the de Sitter points given in Table1 are stable de Sitter points. The conditions for graviton to be of non-ghost nature and scalar field ϕ to be non techyonic are $f_{,R} > 0$ and $f_{,RR} > 0$ respectively. They are investigated for the model in Eq. (2) and it is found that both

n	b	βR_d
1.75	1.021	2.4092
1.75	1.1	2.7777
1.75	1.5	4.2708
1.75	2.0	5.9530
1.75	3.0	9.1930
1.0	2.0	5.1397
0.98	5.0	14.6369

Table 1: de Sitter points for different values of b and n

the conditions are satisfied by all parameter values mentioned in Table1 for $R_d < R < \infty$.
Using Eq. (6) and (7) we can define a potential

$$V(R) = -\frac{Rf(R)}{3} + \int^R f(R^\star)dR^\star, \tag{8}$$

such that $\frac{dV(R)}{dR} = \frac{2f(R)-Rf_{,R}}{3} = 0$ for the minimum at the de Sitter point. The potential for the choice of parameters shown in Table 1 is shown in Fig. 2.

2.2 Fixed Point Analysis

It is necessary to carry out fixed point analysis in order to check whether given model can give rise to dark energy dominated era preceded by matter dominated era or not. Here, we follow the procedure followed by many authors and originally proposed in [20]. Assuming background spacetime as a spatially flat FLRW spacetime, field equations can be written as evolution equations in terms of R, $\dot{R}$, Hubble constant H and matter density ρ_m. These evolution equations can be further written as a set of dynamical system equations by defining dimensionless variables $y_1 \equiv -\dot{f_{,R}}/Hf_{,R}$, $y_2 \equiv -f/6f_{,R}H^2$, and $y_3 \equiv R/6H^2$. Basically, this dynamical system can be characterized by two quantities

$$m \equiv \frac{Rf_{,RR}}{f_{,R}} = \frac{2bn^2x^{3n-1} - bn(n-1)x^{n-1}(1+x^{2n})}{(1+x^{2n})(1+x^{2n}-bnx^{n-1})}, \tag{9}$$

$$r \equiv -\frac{Rf_{,R}}{f} = \frac{y_3}{y_2} = \frac{-x - x^{2n+1} + bnx^n}{(1+x^{2n})(x - b\arctan(x^n))}, \tag{10}$$

where $x = \beta R$. Solving a set of dynamical system equations one can obtain several fixed points namely P_1, P_2, P_3, P_4, P_5 and P_6. As described in [20], there are two fixed points P_1 and P_6 which give rise to late-time cosmic acceleration. The former is de Sitter point. The saddle matter era is realized by fixed point P_5. In Fig.3, $m(r)$ curve is plotted on (r, m) plane for the function given in Eq. (2). The points P_5 and P_6 exist on $m = -r - 1$ line. The condition for the existence of point P_5 is $m(r) = +0,\ dm/dr > -1$, at $r = -1$. If we take limit $\beta R \to \infty$ in expression of r in Eq. (10) we can obtain $r \to -1$. Calculating dm/dr from $(dm/dR)/(dr/dR)$ and taking $R \to \infty$ limit in it, one can end up with $dm/dr(r = -1) \simeq > -1$. This says that P_5 is a saddle point showing existence of saddle matter era in our model at very large curvature. The stability condition for the point P_6 is $m = -r - 1, (\sqrt{3}-1)/2 < m < 1$ which is not satisfied as evident from the Fig.3. Lastly, the de Sitter point P_1, as we have already obtained in Sec.2.1, is a stable point. This can be also proved from its stability condition ($r = -2,\ 0 < m \leq 1$) which is clearly satisfied by our model. Therefore, we can conclude that the model given in Eq. (2) gives the evolution of our universe from saddle matter era (point P_5) to a de Sitter state (point P_1) through blue curve shown in Fig.3 while $m = 0$ line shows the ΛCDM evolution.

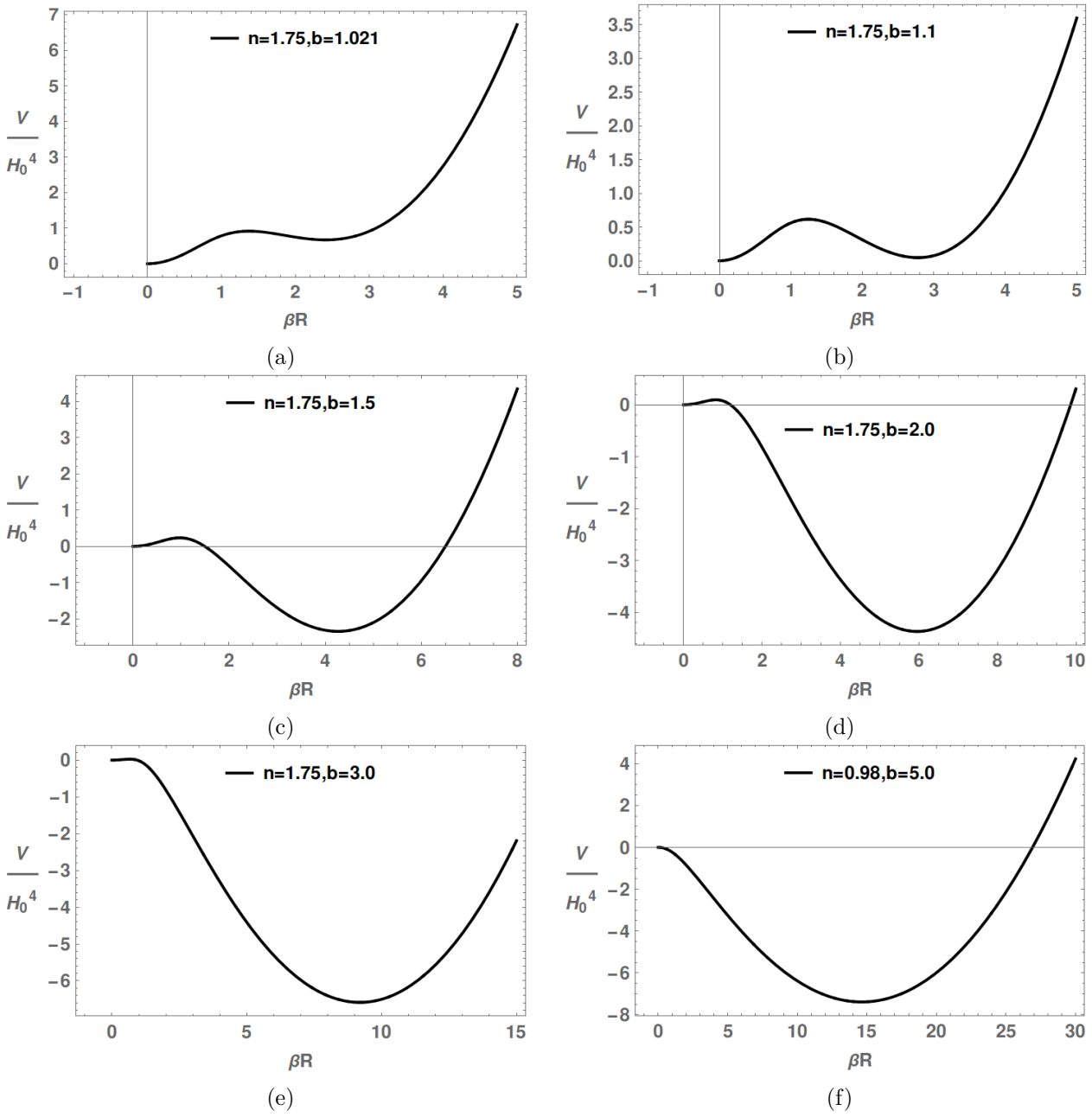

Figure 2: $V(R)/H_0^4$ vs βR for the model (2) and the potential $V(R)$ is defined by Eq. (8)

3 Fifth Force Constraint

It is well-known that the $f(R)$ theory has an extra scalar degree of freedom in addition to usual graviton. Since the scalar field in the theory is a dynamical degree of freedom, it gives rise to a propagating fifth-force which is the cause of the late-time acceleration. But, it must be suppressed at the local gravity scales in order to evade experimental results of solar system tests and EP(Equivalence Principle) violation tests. The condition for the suppression of fifth force on local gravity scales is given by $m_\phi^2 L_s^2 >> 1$, where m_ϕ is the mass of the scalar field and L_s is the typical length scale involved in experiment [43, 44]. One can calculate the value of m_ϕ^2 for our model given in (2), which comes out to be of the order of $10^{-51}m^{-2}$. Considering $L_s = 1m$, the above condition can be seen to be completely violated.

In the Einstein frame, the scalar field of an $f(R)$ theory is a chameleon like field which exhibits

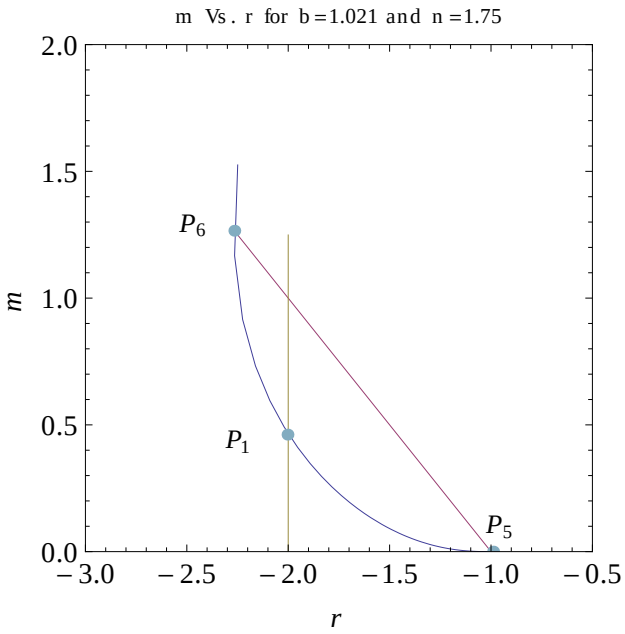

Figure 3: m Vs. r for $n = 1.75$ and $b = 1.021$.

chameleon mechanism given by [24]. The name owes to the fact that the "chameleon" field blends with the environment in the highly densed background and becomes invisible to any experimental searches for fifth-force. This is because the mass of the field depends on the background density. It can be shown as following. The action in Eq. (1) can be written, via a conformal transformation, in Einstein frame as

$$S = \int d^4x\sqrt{-\tilde{g}}\left[\frac{\tilde{R}}{2\kappa^2} - \frac{1}{2}(\tilde{\nabla}\psi)^2 - V_E(\psi) + \mathfrak{L}_m(\tilde{g}_{\mu\nu}e^{-\frac{2}{\sqrt{6}}\kappa\psi})\right]. \tag{11}$$

Here, all quantities having tilde are defined in Einstein frame. The scalar field ψ is related to function $f(R)$ by the relation $\kappa\psi = \sqrt{3/2}\ln f_{,R}$. Let us consider the spherically symmetric body with radius $\tilde{r}_c$. Varying action in (11) w.r.t. ψ we obtain the field equation for ψ as

$$\frac{d^2\psi}{d\tilde{r}^2} + \frac{2}{\tilde{r}}\frac{d\psi}{d\tilde{r}} - \frac{dV_{eff}}{d\psi} = 0. \tag{12}$$

The effective potential V_{eff} is given by

$$V_{eff}(\psi) = V_E(\psi) + e^{-\frac{2}{\sqrt{6}}\kappa\psi}\rho^*. \tag{13}$$

Because of the interplay of two terms self-interaction potential V_E and conformal coupling to the matter, the effective potential posseses the global minimum. By solving the dynamical equation (12), one can find that the scalar field ψ is frozen at the potential minimum with very small magnitude and its mass is very high. Thus, its contribution to the outside field is negligible except for a thin shell regime near the surface of the object. The thin-shell condition is given by

$$\frac{\delta\tilde{r}_c}{\tilde{r}_c} = -\frac{\psi_{out} - \psi_{in}}{\sqrt{6}\Phi_c}. \tag{14}$$

Where, Φ_c is the gravitational potential on the surface of the test body (Sun/Earth) and $\delta\tilde{r}_c$ is the thickness of the thin shell. Here, ψ_{out} and ψ_{in} are value of the field at the minima of V_{eff} outside and inside the body respectively. If $\psi_{in} << \psi_{out}$ the the thin-shell condition written in Eq.(14) can be reduced to

$$|\psi_{out}| \simeq \sqrt{6}\Phi_c\frac{\delta\tilde{r}_c}{\tilde{r}_c}. \tag{15}$$

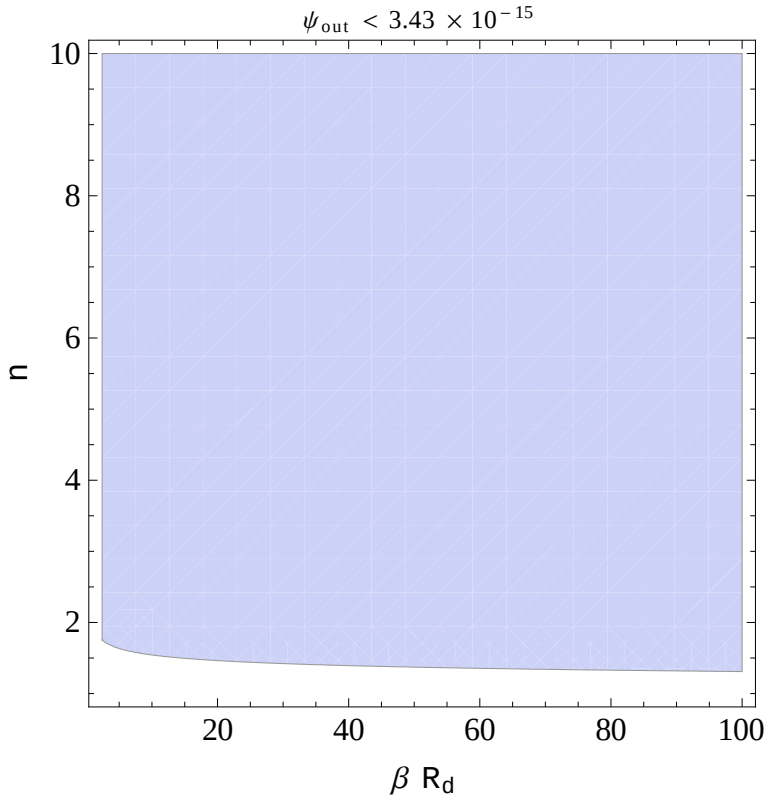

Figure 4: Shaded region is the allowed region for different values of parameter n and βR_d.

The experimental results of the solar system tests and the EP violation tests put the constraints on the r.h.s. of the Eq. (15):

$$|\psi_{out}| \lesssim \begin{cases} 5.97 \times 10^{-11} & \text{(Solar system test)}, \\ 3.43 \times 10^{-15} & \text{(Equivalence Principle (EP) test)}. \end{cases} \tag{16}$$

For the model given in (2), ψ_{out} can be written as

$$\psi_{out} \approx \frac{\sqrt{6}}{2} F_{,R}|_{R=\rho_{out}} = \frac{\sqrt{6}}{2} \left[-nb \frac{(\beta\rho_{out})^{n-1}}{\{1+(\beta\rho_{out})^{2n}\}} \right]. \tag{17}$$

Here, we have considered the approximation that $R >> 1/\beta$. Let us put $\beta\rho_{out} = \beta R_d \frac{\rho_{out}}{R_d}$. Since $\rho_{out} \simeq 10^{-24} g/cm^3$ and $R_d \simeq \rho_c \sim 10^{-29} g/cm^3$ one can write $\beta\rho_{out} \simeq \beta R_d \times 10^5$ in Eq. (17).

$$\psi_{out} \approx \frac{\sqrt{6}}{2} \left[-nb \frac{(\beta R_d \times 10^5)^{n-1}}{\{1+(\beta R_d \times 10^5)^{2n}\}} \right] \tag{18}$$

From the de Sitter condition in Eq. (7), parameter b can be written in terms of n and βR_d as

$$b = \frac{-\beta R_d}{-2\arctan(\beta R_d)^n + \frac{n(\beta R_d)^n}{1+(\beta R_d)^{2n}}}. \tag{19}$$

Plugging Eq. (19) into Eq. (18) one ends up with the expression

$$|\psi_{out}| \approx \left| \frac{-n\sqrt{6}}{2} \left(\frac{-\beta R_d}{-2\arctan(\beta R_d)^n + \frac{n(\beta R_d)^n}{1+(\beta R_d)^{2n}}} \right) \frac{(\beta R_d \times 10^5)^{n-1}}{\{1+(\beta R_d \times 10^5)^{2n}\}} \right| \tag{20}$$

With the help of Eq. (20) and Eq. (16) we can put the constraint on our model parameters to evade the fifth-force constraint. Fig.4 exhibits allowed regions for different values of parameter n and βR_d. From the Fig.4, one can conclude that $b \geq 1.021$ and $n \geq 1.75$ to evade the local gravity test. The corresponding de Sitter point βR_d has to be ≥ 2.4.

4 Curvature Singularity

The trace equation (5) can also be written as

$$3\Box F_{,R}(R) - 2F - R + RF_{,R}(R) = \kappa^2 T \tag{21}$$

Rewriting the term $\Box F_{,R} = \Box\phi$, where ϕ is the scalar field in the jordan frame, one can write equation of motion for ϕ as

$$\Box\phi = \frac{dV_J}{d\phi} + \frac{\kappa^2}{3}T, \tag{22}$$

where

$$\frac{dV_J}{d\phi} = \frac{1}{3}(R + 2F - RF_{,R}). \tag{23}$$

Here, V_J is the scalar field potential in the jordan frame. For the model written in (2), $dV_J/d\phi$ can be written as

$$\frac{dV_J}{d\phi} = \frac{1}{3}\left[-2\frac{b}{\beta}\arctan(\beta R(\phi))^n + R + \frac{b}{\beta}\frac{n(\beta R(\phi))^n}{1+(\beta R(\phi))^{2n}}\right] \tag{24}$$

The dynamics of the scalar field ϕ depends solely on the potential V_J in vacuum. While in the presence of matter, the term $\kappa^2 T$ will also play a role. In this case the equation of motion can be written as

$$\Box\phi = \frac{\partial V_J^{eff}}{\partial\phi}, \tag{25}$$

where

$$\frac{\partial V_J^{eff}}{\partial\phi} = \frac{1}{3}(R + 2F - RF_{,R} + \kappa^2 T). \tag{26}$$

If we integrate the Eq. (24) with respect to ϕ, we obtain $V_J(R(\phi))$. The minimum of the potential V_J

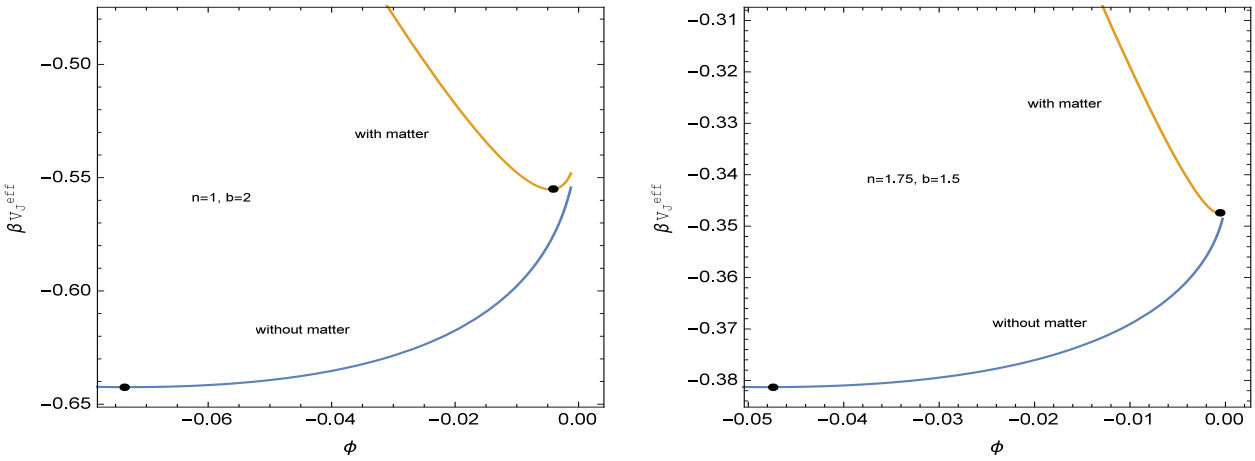

(a) $n = 1,\ b = 2$ (b) $n = 1.75,\ b = 1.5$

Figure 5: βV_J^{eff} Vs. ϕ

corresponds to the de Sitter point in the vacuum about which the field ϕ oscillates. This minimum can be at finite distance in ϕ and with finite potential difference from the singular point $\phi = 0$. At the singular point $\phi = 0$, The scalar curvature R becomes infinity and therefore it is called curvature singularity.

The plots for $V_J^{eff}(\phi)$ with matter and without matter are shown for different values of parameters n and b in figures 5 and 6. The yellow and blue curves are drawn with matter and without matter respectively. The black dots are minima of the potential V_J^{eff}. It can be easily seen that the minimum moves closer to the singularity in the presence of matter thus making the scalar field more vulnerable

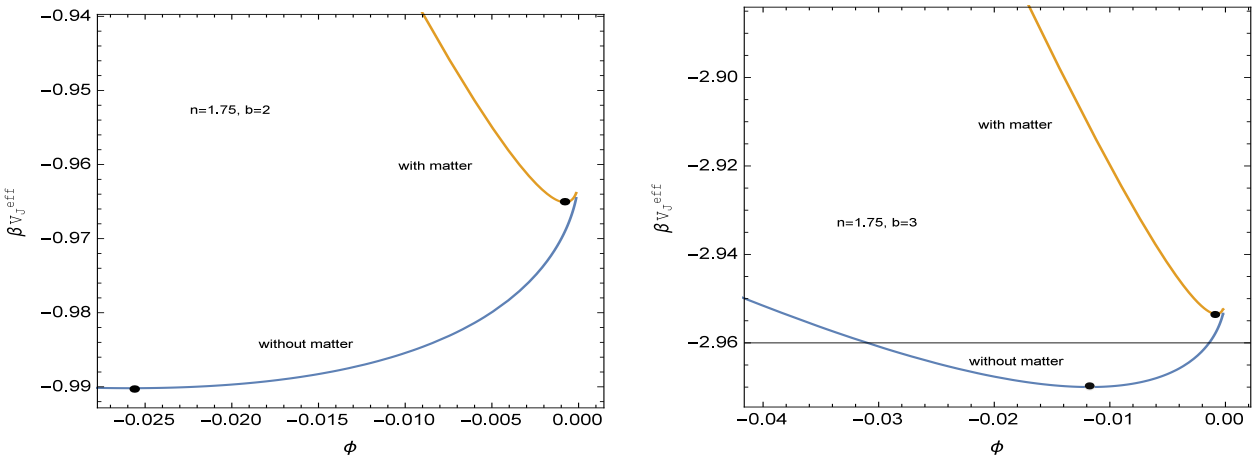

(a) $n = 1.75,\ b = 2$ (b) $n = 1.75,\ b = 3$

Figure 6: βV_J^{eff} Vs. ϕ

to meet the singularity. It is also clear from the figures5b and 6 that the de Sitter minima shift more towards the singularity as b increases. The minimum is at closer distance for larger values of n as evident from the figures 5a and 6a. Therefore the arctan model is safer than our model in (2) but not free from fatal curvature singularity at all. But, the curvature singularity can be cured by adding R^2 term to the lagrangian since it can increase the value of potential V_J to the infinity as ϕ approaches the singularity for fine tunned parameter values as suggested in [11].

5 Cosmological Evolution

In this section we discuss cosmological implications of model given in Eq. (2). We consider homogeneous and isotropic FRW universe described by the metric

$$ds^2 = -dt^2 + a^2(t)\left[\frac{dr^2}{1-Kr^2} + r^2\left(d\theta^2 + \sin^2\theta d\phi^2\right)\right] \tag{27}$$

Using Eq. (6) with above spacetime we get

$$\ddot{R} = -3H\dot{R} - \frac{1}{3f_{,RR}}\left[3f_{,RRR}\dot{R}^2 + 2f - f_{,R}R + \kappa^2 T\right] \tag{28}$$

The cosmological evolution can be obtained by solving field equation Eq. (4) with FRW metric and diagonal energy-momentum tensor. The equations governing the scale factor and Hubble constant H for flat FRW universe are given as

$$H^2 + \frac{1}{f_{,R}}\left[f_{,RR}H\dot{R} - \frac{1}{6}\left(f_{,R}R - f\right)\right] = -\frac{\kappa^2 T_t^t}{3f_{,R}}, \tag{29}$$

$$\dot{H} = -H^2 + \frac{1}{f_{,R}}\left(f_{,RR}H\dot{R} + \frac{f}{6} + \frac{\kappa^2 T_t^t}{3}\right), \tag{30}$$

where $H = \frac{\dot{a}}{a}$. The expression for the Ricci scalar in terms of Hubble constant directly obtained from the metric is given by

$$R = 6\left(\dot{H} + 2H^2 + \frac{k}{a^2}\right) \tag{31}$$

The energy-momentum tensor considered for cosmological evolution has three contributions i.e. baryon, radiation and dark matter. The conservation equation $\nabla_a T^{ab} = 0$, satisfied by each component separately, leads to the following equation,

$$\dot{\rho}_T + 3H\left(\rho_t + p_t\right) = 0. \tag{32}$$

Here the total energy density is $\rho_T = \rho_{bar} + \rho_{DM} + \rho_{rad}$. The above equation can be integrated by using p_{bar}, $p_{DM} = 0$ and $p_{rad} = \rho_{rad}/3$ and the energy density can be expressed in terms of scale factor as

$$\rho_T = \frac{\rho^0_{bar} + \rho^0_{DM}}{(a/a_0)^3} + \frac{\rho^0_{rad}}{(a/a_0)^4}, \tag{33}$$

where the knotted quantities indicate their values today. The time-time component of the energy-momentum tensor and its trace appearing in equations (28), (29) and (30) can be written in terms of energy density and pressure as $T^t_t = -\rho_T$ and $T = -(\rho_{bar} + \rho_{DM})$

Now to obtain the equation of state of $f(R)$ gravity one can define the energy density ρ_X such that the Friedmann equation (29) looks like

$$H^2 = \frac{\kappa^2}{3}(\rho + \rho_X). \tag{34}$$

Similarly the pressure p_X can also be defined in a way so that the Eq. (30) will become

$$\dot{H} + H^2 = -\frac{\kappa^2}{6}(\rho + \rho_X + 3(p_{rad} + p_X)). \tag{35}$$

Now using the above two equations along with Eq. (29) and Eq. (30) the energy density and pressure for $f(R)$ fluid can be written as

$$\rho_X = \frac{1}{\kappa^2 f_{,R}}\left[\frac{1}{2}(f_{,R}R - f) - 3f_{,RR}H\dot{R} + \kappa^2\rho(1 - f_{,R})\right], \tag{36}$$

$$p_X = -\frac{1}{3\kappa^2 f_{,R}}\left[\frac{1}{2}(f_{,R}R + f) + 3f_{,RR}H\dot{R} - \kappa^2(\rho - 3p_{rad}f_{,R})\right]. \tag{37}$$

With these expressions of energy density and pressure we can write the equation of state for $f(R)$ as

$$w_X = \frac{p_X}{\rho_X}. \tag{38}$$

The equation of state w_X can also be written in the following form by using Eq. (34), (35) and (31) as

$$w_X = \frac{3H^2 - 3\kappa^2 p_{rad} - R}{3(3H^2 - \kappa^2\rho)}. \tag{39}$$

To obtain the behavior of R and H w.r.t redshift z we solve Eqns.(28), (29), (30) and (31) numerically using the method described in [41]. To integrate these differential equations we chose

$$\alpha = \ln(a/a_0) \tag{40}$$

as an independent variable instead of t. Eqns. (28), (29), (30) and (31) can be expressed in terms of α as

$$R'' = -R'\left(1 + \frac{R}{6H^2}\right) - \frac{1}{3f_{,RR}H^2}\left[3f_{,RRR}H^2R'^2 + 2f - f_{,R}R + \kappa^2 T\right], \tag{41}$$

$$H' = -2H + \frac{R}{6H}, \tag{42}$$

$$H^2 + \frac{1}{f_{,R}}\left[f_{,RR}H^2R' - \frac{1}{6}(f_{,R}R - f)\right] = -\frac{\kappa^2 T^t_t}{3f_R}, \tag{43}$$

$$H' = -H + \frac{1}{f_{,R}H}\left(f_{,RR}H^2R' + \frac{f}{6} + \frac{\kappa^2 T^t_t}{3}\right). \tag{44}$$

To numerically integrate the above differential equations we can use either Eq. (42) or (44) for H. To check the consistency of the code we have used both. Eq. (43) is modified Hamiltonian constraint

and can be used to determine the accuracy of the code. The initial conditions for R and H are taken as described in [41].

The behavior of Ricci scalar R and Hubble constant H is depicted in Fig. 7 to 12 for the choice of the parameters given in Table 1. The Ricci scalar oscillates around its value at the de Sitter point today, which can be seen by applying linear perturbations (see Fig. 2) around the de Sitter minimum. The Hubble constant today also oscillates. From Fig. 11 we see that the oscillations are not significant for larger value of b with $n = 1.75$.

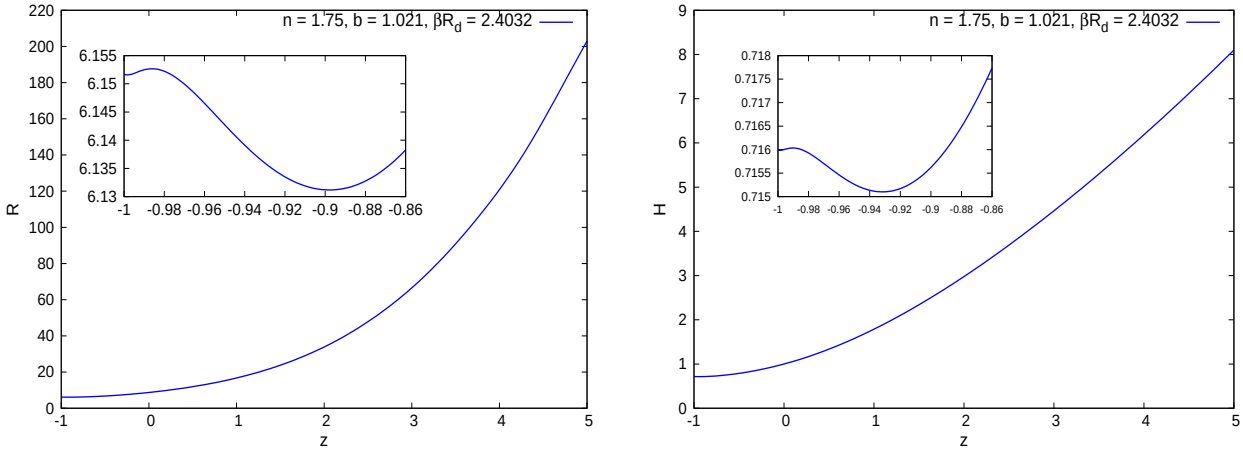

(a) R vs z (b) H vs z

Figure 7: Variation of Ricci scalar and expansion rate w.r.t z for the model (2)

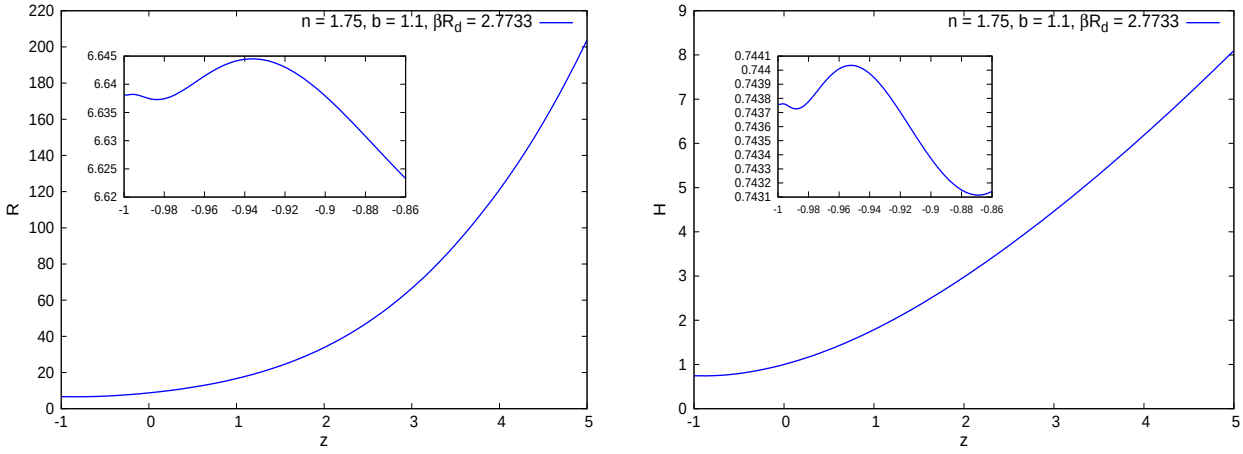

(a) R vs z (b) H vs z

Figure 8: Variation of Ricci scalar and expansion rate w.r.t z for the model (2)

The dimensionless densities for different species can be expressed as

$$\Omega := \Omega_{rad} + \Omega_{bar} + \Omega_{DM} + \Omega_X = 1, \tag{45}$$

where $\Omega_i = \frac{\kappa\rho_i}{3H^2}$. The density for the $f(R)$ model is given by (36). The variation of matter density Ω_M and the density of $f(R)$ model (2) Ω_X w.r.t z is shown in Fig. 13 for the values of n and b given in Table 1. We have also plotted the same densities for the ΛCDM model for reference. The various density parameters Ω_i for the ΛCDM model can be expressed in terms of their values today as

$$\Omega_i^{\Lambda CDM} = \frac{\Omega_i^{0\,\Lambda CDM}\bar{a}^I}{\left[\left(\Omega_{bar}^{0\,\Lambda CDM} + \Omega_{DM}^{0\,\Lambda CDM}\right)\bar{a}^{-3} + \Omega_{rad}^{0\,\Lambda CDM}\bar{a}^{-4} + \Omega_\Lambda^0\right]}. \tag{46}$$

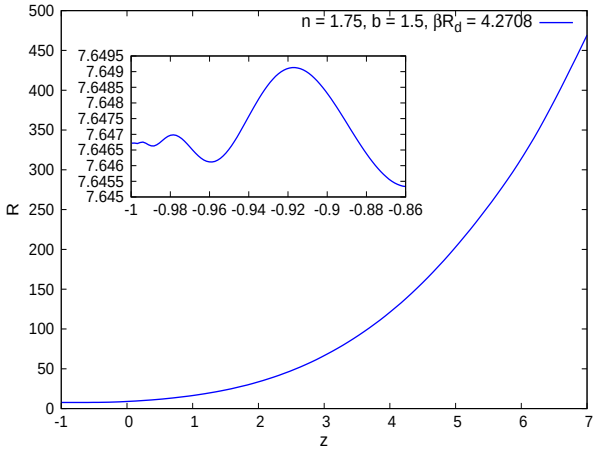

(a) R vs z

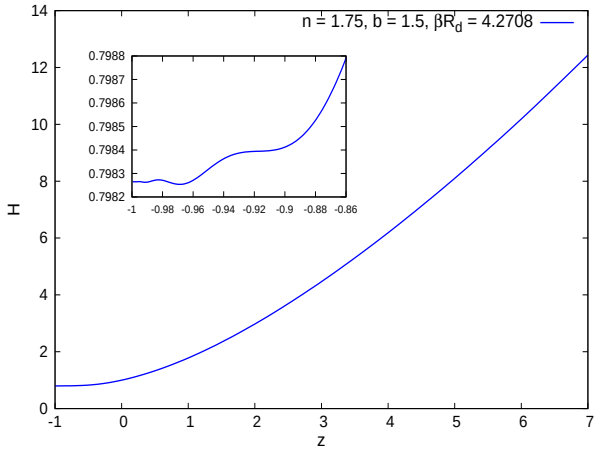

(b) H vs z

Figure 9: Variation of Ricci scalar and expansion rate w.r.t z for the model (2)

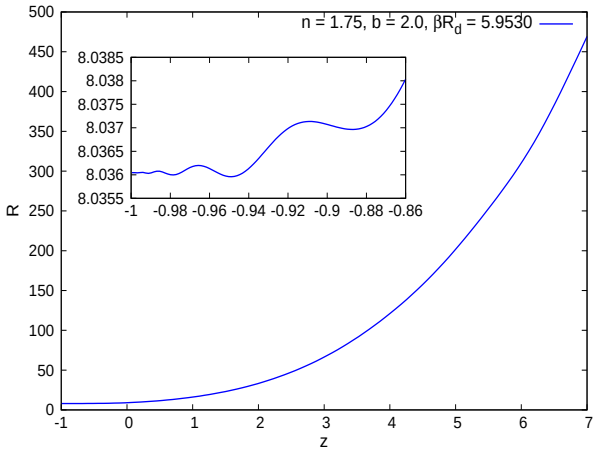

(a) R vs z

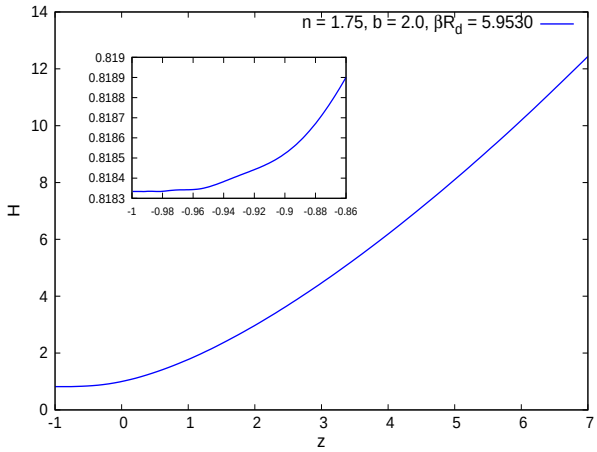

(b) H vs z

Figure 10: Variation of Ricci scalar and expansion rate w.r.t z for the model (2)

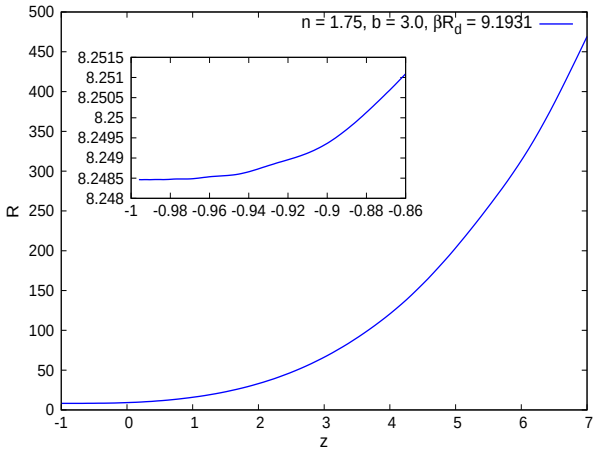

(a) R vs z

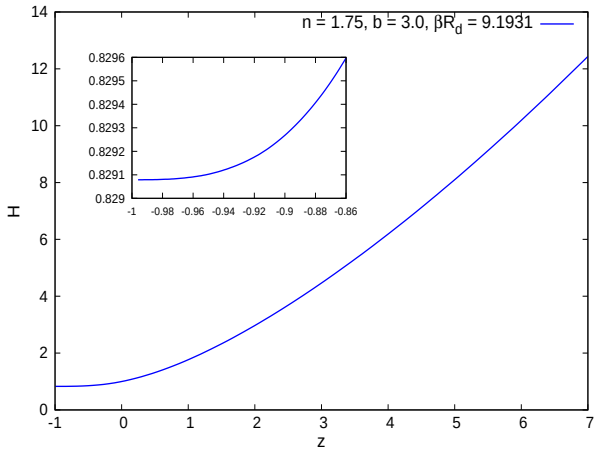

(b) H vs z

Figure 11: Variation of Ricci scalar and expansion rate w.r.t z for the model (2)

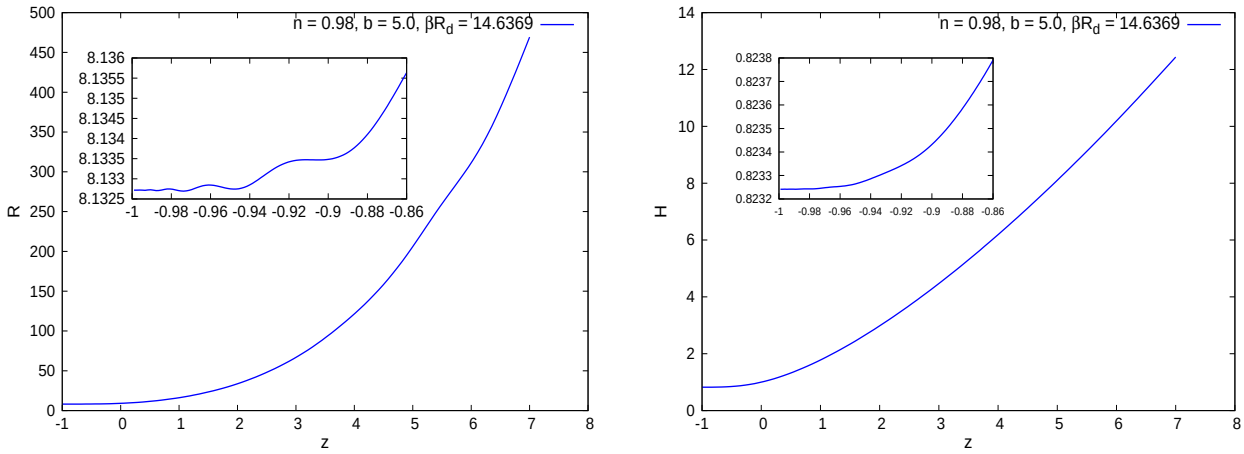

(a) R vs z (b) H vs z

Figure 12: Variation of Ricci scalar and expansion rate w.r.t z for the model (2)

Here i represents baryon, dark matter, radiation and Λ and $I = -3, -3, -4, 0$ for these species respectively. It is clear from the Fig. 13 that the variation of Ω_i w.r.t z is not much different for all the choices of the parameters n and b and for $n = 1.75$ and $b = 3.0$ the model is more closer to ΛCDM. It is also clear from the Fig. 13 that the $f(R)$ model (2) presented in this work exhibit sufficiently long matter dominated era as predicted by fixed point analysis presented in Sec. 2.2. For larger redshift Ω_X behaves in a similar way as Ω_Λ so we expect a radiation era in the early universe similar to ΛCDM model so that the predictions of Nucleosynthesis are nor spoiled.

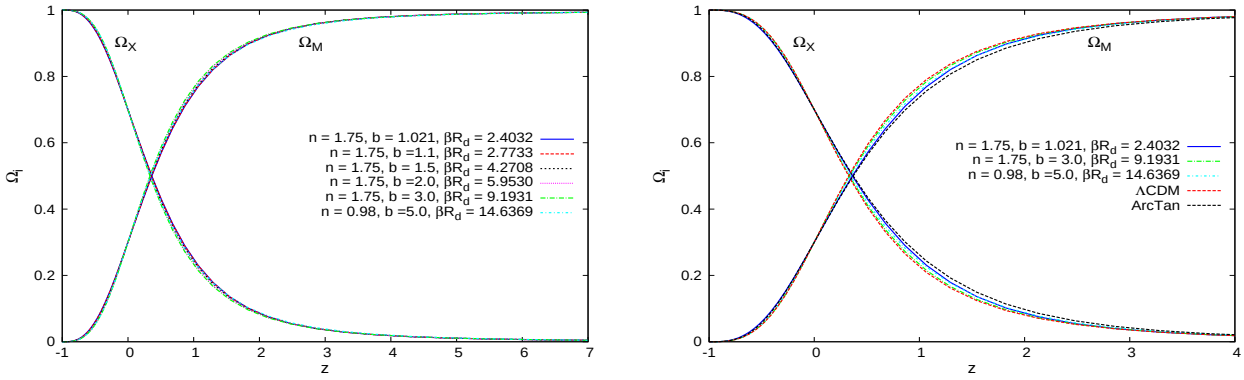

(a) Ω_i vs z (b) Ω_i vs z

Figure 13: Variation of Ω_i w.r.t z. The density parameter Ω_X for the model (2) is given by $\Omega_X = \frac{\kappa\rho_X}{3H^2}$, where ρ_X is given by Eq. (36).

Fig. 14 shows the behavior of equation of state of the $f(R)$ component of the fluid given by (2) and the equation of state of the total fluid. From Fig. [14a] we see that the equation of state for the $f(R)$ model (2) exhibits oscillation around phantom divide $\omega = -1$ for all choice of parameters. The existence of matter era for higher redshifts can also be seen from the behavior of ω_{total} as depicted in Fig. 14b.

6 Luminosity distance and distance modulus

The observational evidence for dark energy comes from measuring luminosity distance to supernovae (SNIa). We can use the same supernovae data to constrain our new model of $f(R)$ theory. The

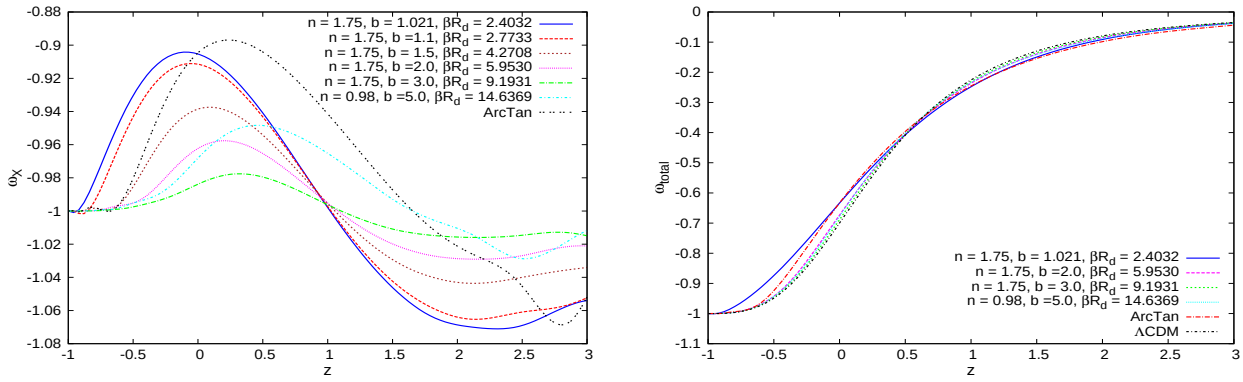

(a) ω_X vs z (b) ω_{total} vs z

Figure 14: Equation of state ω_X given by Eq. (39) and ω_{total} w.r.t z

luminosity distance is given by

$$d_L = \frac{\zeta(\bar{a})}{\bar{a}}, \tag{47}$$

where $\bar{a} = \frac{a}{a_0}$ and

$$\zeta = cH_0^{-1} \int_{\bar{a}}^{1} \frac{d\bar{a}^\star}{\bar{a}^{\star 2} \bar{H}(\bar{a}^\star)}. \tag{48}$$

Here speed of light has been introduced explicitly in order to compute distance in units of Mpc and $\bar{H} = \frac{H}{H_0}$. In order to compute ζ by the numerical method described in [41] we can transform the expression (48) in terms of differential equation

$$\frac{d\bar{\zeta}}{d\bar{a}} = -\frac{1}{\bar{a}^2 \bar{H}(\bar{a})}, \tag{49}$$

where $\bar{\zeta} = \frac{\zeta}{(cH_0^{-1})}$ is dimensionless and the above differential equation in terms of variable $\alpha = \ln(\bar{a})$ can be written as

$$\bar{\zeta}' = -\frac{e^{-\alpha}}{\bar{H}}. \tag{50}$$

The solution for the above differential equation can be obtained simultaneously with the field equations and the initial condition for ζ is chosen as described in [41]. The distance modulus given by

$$\mu = m - M = 5 \log_{10} \frac{d_L^{flat}}{Mpc} + 25 \tag{51}$$

is the quantity reported by supernovae data.

Fig.15 shows variation of luminosity distance and distance modulus w.r.t z for the $f(R)$ model (2) along with the ΛCDM. The luminosity distance and distance modulus for the model is not much different from the ΛCDM for all choice of parameters. Distance modulus is also plotted along with the supernovae data of UNION 2 [42].

7 Conclusions

To cure the incompetence of the arctan model proposed in [19] to evade the local gravity tests [1], we extend the model to a new model given in Eq. (2). Here, we show that our model can pass local gravity tests, and constrain the model parameters for fifth-force condition to be hold.

The model written in (2) can mimick as an effective cosmological constant plus GR when curvature of the universe is very large. As depicted in Fig. 1, taking large value of power n can make the function

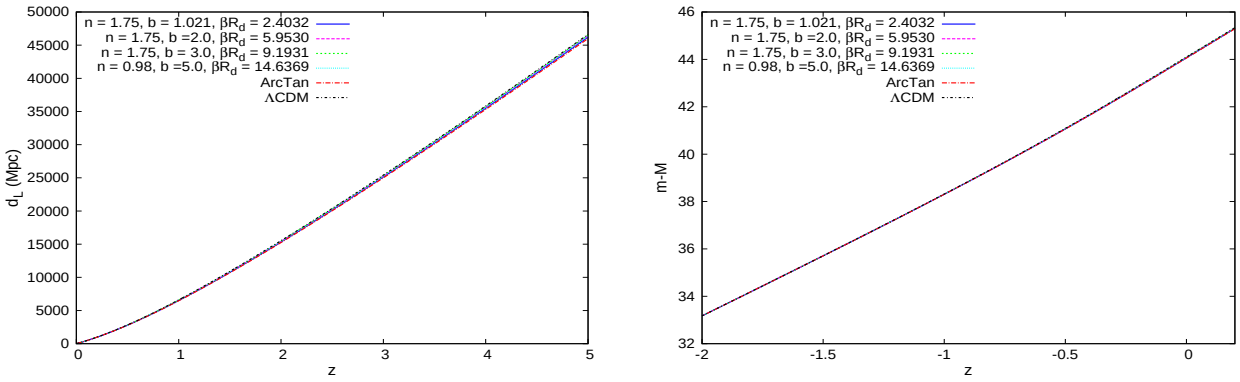

(a) Luminosity distance vs z

(b) Distance modulus vs z

Figure 15: d_L and $m - M$ vs z for $f(R)$ model with various choice of parameters along with the ΛCDM.

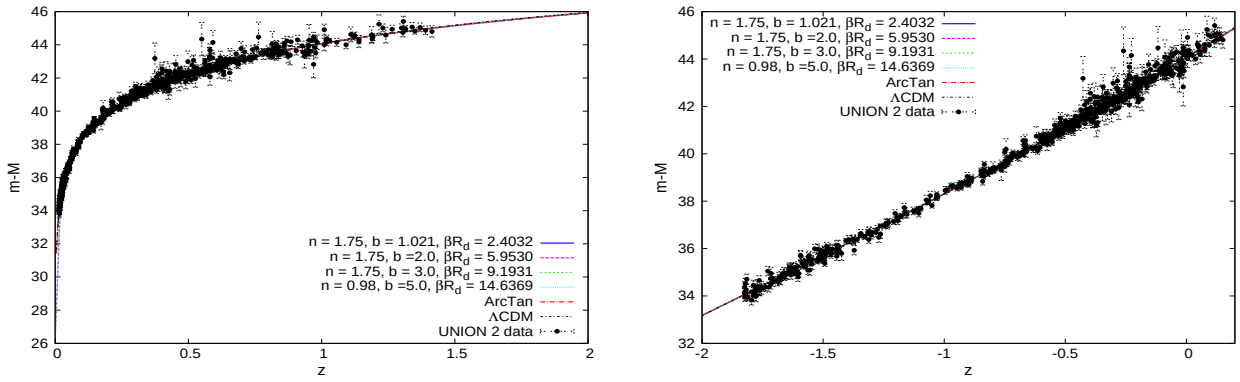

(a)

(b)

Figure 16: Distance modulus for the model (2) along with the UNION 2 data of [42]

$F(R)$ increases more rapidly to a constant value therefore the proper range of n should be $1 < n \leq 2$. We also find that the stable fixed points of the model are P_5 and P_1 exhibiting the evolution of the universe fron saddle matter era to late-time acceleration.

We put the model in (2) under scrutiny to investigate the fifth-force constraints for the model through chameleon mechanism. We find that the model can evade the local gravity test for the parameter values $n \geq 1.75$ and $b \geq 1.021$. These constraints on the parameter values give rise to constraint on the value of corresponding de Sitter point which is $\beta R_d \geq 2.4$.

We also investigate the existence of curvature singularity in the model in Eq. (2). We find that there may be finite probability for scalar field to hit the singularity due to to the finite potential V_J at the singular point. As described in Ref. [11], the curvature singularity can be cured by adding R^2 term to the lagrangian.

We also derive the cosmological evolution equations for this model considering an FRW background universe and solve them numerically. We obtain the oscillatory behavior of Ricci scalar R and Hubble parameter H which becomes less pronounced with higher values of b. It is found that the model (2) provides sufficiently long matter dominated era and radiation era at larger redshifts similar to ΛCDM model. These results are reconciled with the predictions of fixed point analysis and nucleosynthesis. The equation of state of the $f(R)$ component of the fluid w_x for our model oscillates around phantom divide $w = -1$.

We also find that our model is barely distinguishable from ΛCDM model from the perspective of luminosity distance and distance modulus. But, this can not be a decisive statement because the distinguishability of any $f(R)$ model from ΛCDM model may be better tested with large scale

structure data. Thus, we conclude that the model given in Eq. (2) gives rise to the dark energy dominated era while having correct cosmic history to coinside with other cosmological observations and also evade local gravity tests.

References

[1] K. Dutta, S. Panda and A. Patel, arXiv:1601.07928 [gr-qc] (accepted for publication in PRD).

[2] A. G. Riess *et al.* [Supernova Search Team Collaboration], Astron. J. **116**, 1009 (1998) [astro-ph/9805201]. S. Perlmutter *et al.* [Supernova Cosmology Project Collaboration], Nature **391**, 51 (1998) [astro-ph/9712212]. B. P. Schmidt *et al.* [Supernova Search Team Collaboration], Astrophys. J. **507**, 46 (1998) [astro-ph/9805200]. S. Perlmutter *et al.* [Supernova Cosmology Project Collaboration], Astrophys. J. **517**, 565 (1999) [astro-ph/9812133]. A. G. Riess *et al.* [Supernova Search Team Collaboration], Astrophys. J. **607**, 665 (2004) [astro-ph/0402512].

[3] A. Padilla, arXiv:1502.05296 [hep-th].

[4] A.D.Felice and S.Tsujikawa, Living Rev. Relativity, 13, (2010), 3.

[5] S. Capozziello and M. De Laurentis, Phys. Rept. **509**, 167 (2011) [arXiv:1108.6266 [gr-qc]].

[6] T. P. Sotiriou and V. Faraoni, Rev. Mod. Phys. **82**, 451 (2010) [arXiv:0805.1726 [gr-qc]].

[7] S. Nojiri and S. D. Odintsov, Phys. Rept. **505**, 59 (2011) [arXiv:1011.0544 [gr-qc]].

[8] A. Starobinsky, JETP Lett. **86**, 157 (2007) [0706.2041]

[9] W. Hu and I. Sawicki, Phys. Rev. D **76**, 064004 (2007) [arXiv:0705.1158 [astro-ph]].

[10] S. A. Appleby and R. A. Battye, Phys. Lett. B **654**, 7 (2007) [arXiv:0705.3199 [astro-ph]].

[11] S. Appleby, R. Battye and A. Starobinsky JCAP **1006**, 005 (2010) [astro-ph/0909.1737]

[12] S. Tsujikawa, Phys. Rev. D **77**, 023507 (2008) [arXiv:0709.1391 [astro-ph]].

[13] P. Zhang, Phys. Rev. D **73**, 123504 (2006) [astro-ph/0511218].

[14] G. Cognola, E. Elizalde, S. Nojiri, S. D. Odintsov, L. Sebastiani and S. Zerbini, Phys. Rev. D **77**, 046009 (2008) [arXiv:0712.4017 [hep-th]].

[15] V. Miranda, S. E. Joras, I. Waga and M. Quartin, Phys. Rev. Lett. **102**, 221101 (2009) doi:10.1103/PhysRevLett.102.221101 [arXiv:0905.1941 [astro-ph.CO]].

[16] E. V. Linder, Phys. Rev. D **80**, 123528 (2009) [arXiv:0905.2962 [astro-ph.CO]].

[17] K. Bamba, C. Q. Geng and C. C. Lee, JCAP **1008**, 021 (2010) [arXiv:1005.4574 [astro-ph.CO]].

[18] K. Bamba, C. Q. Geng and C. C. Lee, Int. J. Mod. Phys. D **20**, 1339 (2011) [arXiv:1108.2557 [gr-qc]].

[19] S. I. Kruglov, Phys. Rev. D **89**, no. 6, 064004 (2014) [arXiv:1310.6915 [gr-qc]].

[20] L. Amendola, R. Gannouji, D. Polarski and S. Tsujikawa, Phys. Rev. D **75**, 083504 (2007) [gr-qc/0612180].

[21] S. Carloni, JCAP **1509**, no. 09, 013 (2015) [arXiv:1505.06015 [gr-qc]].

[22] S. Kandhai and P. K. S. Dunsby, arXiv:1511.00101 [gr-qc].

[23] C. M. Will, Living Rev. Rel. **17**, 4 (2014) [arXiv:1403.7377 [gr-qc]].

[24] J. Khoury and A. Weltman, Phys. Rev. Lett. **93**, 171104 (2004) [astro-ph/0309300]; J. Khoury and A. Weltman, Phys. Rev. D **69**, 044026 (2004) [astro-ph/0309411].

[25] S. Capozziello, S. Tsujikawa, Phys. Rev. D **77**, 107501 (2008) [gr-qc/0712.2268]

[26] S. A. Appleby and R. A. Battye, JCAP **0805**, 019 (2008) [arXiv:0803.1081 [astro-ph]].

[27] A. Frolov, Phys. Rev. Lett. **101**, 061103 (2008) [astro-ph/0803.2500]

[28] K. Dutta, S. Panda and A. Patel, Phys. Rev. D **92**, no. 6, 063503 (2015) [arXiv:1504.05790 [gr-qc]].

[29] S. Nojiri and S. D. Odintsov, Phys. Rev. D **78**, 046006 (2008) [arXiv:0804.3519 [hep-th]].

[30] K. Bamba, S. Nojiri and S. D. Odintsov, JCAP **0810**, 045 (2008) [arXiv:0807.2575 [hep-th]].

[31] A. Dev, D. Jain, S. Jhingan, S. Nojiri, M. Sami and I. Thongkool, Phys. Rev. D **78**, 083515 (2008) [hep-th/0807.3445].

[32] I. Thongkool, M. Sami, R. Gannouji and S. Jhingan, Phys. Rev. D **80**, 043523 (2009) [arXiv:0906.2460 [hep-th]].

[33] S. Capozziello, M. De Laurentis, S. Nojiri and S. D. Odintsov, Phys. Rev. D **79**, 124007 (2009) [arXiv:0903.2753 [hep-th]].

[34] A. de la Cruz-Dombriz, P. K. S. Dunsby, S. Kandhai and D. Saez-Gomez, Phys. Rev. D **93**, no. 8, 084016 (2016) [arXiv:1511.00102 [gr-qc]].

[35] E. Arbuzova, S. Dolgov, Phys. Lett. B **700**, 289 (2011) [astro-ph/1012.1963]

[36] C. Lee, C. Geng and L. Yang, Prog. Theor. Phys. **128**, 415 (2012) [astro-ph/1201.4546].

[37] L. Reverberi, Phys. Rev. D **87**, 084005 (2013) [gr-qc/1212.2870]

[38] T. Kobayashi and K. i. Maeda, Phys. Rev. D **78**, 064019 (2008) [arXiv:0807.2503 [astro-ph]].

[39] A. Upadhye and W. Hu, Phys. Rev. D **80**, 064002 (2009) [arXiv:0905.4055 [astro-ph.CO]].

[40] E. Babichev and D. Langlois, Phys. Rev. D **81**, 124051 (2010) [arXiv:0911.1297 [gr-qc]].

[41] L. G. Jaime, L. Patino and M. Salgado, arXiv:1206.1642 [gr-qc].

[42] R. Amanullah, et al. (Supernova Cosmology Project), Astrophys. J. 716, 712 (2010)

[43] G. J. Olmo, Phys. Rev. D **72**, 083505 (2005) [gr-qc/0505135].

[44] G. J. Olmo, Phys. Rev. Lett. **95**, 261102 (2005) [gr-qc/0505101].